Boundary-Layer Meteorol (2011) 139:61–81
DOI 10.1007/s10546-010-9578-9

ARTICLE

Variability of Sub-Canopy Flow, Temperature, and Horizontal Advection in Moderately Complex Terrain

Christoph K. Thomas

Received: 30 March 2010 / Accepted: 16 December 2010 / Published online: 8 January 2011

Abstract We examine the space–time structure of the wind and temperature fields, as well as that of the resulting spatial temperature gradients and horizontal advection of sensible heat, in the sub-canopy of a forest with a dense overstorey in moderately complex terrain. Data were collected from a sensor network consisting of ten stations and subject to orthogonal decomposition using the multiresolution basis set and stochastic analyses including two-point correlations, dimensional structure functions, and various other bulk measures for space and time variability. Despite some similarities, fundamental differences were found in the space–time structure of the motions dominating the variability of the sub-canopy wind and temperature fields. The dominating motions occupy similar spatial, but different temporal, scales. A conceptual space–time diagram was constructed based on the stochastic analysis that includes the important end members of the spatial and temporal scales of the observed motions of both variables. Short-lived and small-scale motions govern the variability of the wind, while the diurnal temperature oscillation driven by the surface radiative transfer is the main determinant of the variability in the temperature signal, which occupies much larger time scales. This scale mismatch renders Taylor's hypothesis for sub-canopy flow invalid and aggravates the computation of meaningful estimates of horizontal advective fluxes without dense spatial information. It may further explain the ambiguous and inconclusive results reported in numerous energy and mass balance and advection studies evaluating the hypothesis that accounting for budget components other than the change in storage term and the vertical turbulent flux improves the budget closure when turbulent diffusion is suppressed in plant canopies. Estimates of spatial temperature gradients and advective fluxes were sensitive to the network geometry and the spatial interpolation method. The assumption of linear spatial temperature gradients was not supported by the results, and leads to increased spatial and temporal variability of inferred spatial gradients and advection estimates. A method is proposed to estimate the appropriate minimum network size of wind and temperature sensors suitable for an evaluation of energy and mass balances by reducing spatial and temporal

C. K. Thomas (✉)
College of Oceanic and Atmospheric Sciences, Oregon State University, 104 COAS Admin Bldg, Corvallis, OR 97331, USA
e-mail: chthomas@coas.oregonstate.edu

variability of the spatially sampled signals, which was estimated to be on the order of 200 m at the study site.

Keywords Advection · Energy budget · Plant canopies · Sensible heat · Taylor's hypothesis · Variability

1 Introduction

Over the past few decades many micrometeorological and biogeochemical studies have focused on the experimental implementation, analytical evaluation, and interpretation of the principles of conservation of energy and mass commonly applied to quantify land surface–atmosphere exchange, particularly for carbon dioxide (net ecosystem exchange, NEE, e.g. Feigenwinter et al. 2004; Staebler and Fitzjarrald 2004; Aubinet et al. 2005; Aubinet 2008; Leuning et al. 2008), but also for sensible and latent heat (e.g. Paw et al. 2000; Wilson and Baldocchi 2000; Lee and Hu 2002; Moderow et al. 2007). Most studies evaluated the contributions of horizontal and vertical advection, but some also examined the contribution of horizontal flux divergence to the surface energy and mass budgets in plant canopies. Results collectively showed that the inclusion of terms other than the turbulent vertical flux and the change in storage term, the sum of which is commonly used to quantify NEE, does not necessarily close the budgets. However, some studies concluded that the residual may be diminished when including advective contributions to scalar budgets, particularly at night when weak winds in combination with radiative cooling often lead to stable stratification suppressing turbulent diffusion (e.g. Aubinet et al. 2003; Staebler and Fitzjarrald 2004). Patterns in daytime advection were found to be more ambiguous.

Despite these significant advances, particularly for nocturnal observations, little attention has been given to the spatiotemporal variability of the wind and scalars fields, their gradients, and their dependence on the heterogeneity of the sub-canopy architecture in plant canopies. Wilson and Meyers (2001) measured the variability of sub-canopy eddy-covariance fluxes with three vertically or horizontally separated systems, but primarily focused on the variation of the resultant turbulent carbon dioxide, latent, and sensible heat fluxes rather than that of the primary wind and scalars fields. They concluded that the spatial variability of the fluxes decreased with longer temporal averaging. A comprehensive study was conducted by Staebler and Fitzjarrald (2004, 2005) examining the variability of the sub-canopy wind field in Harvard Forest, its connection with local variations of the sub-canopy vegetation representing flow obstructions, and its possible driving mechanisms. Based on measurements of seven sub-canopy sonic anemometers arranged in a square-shaped domain with stations located around the perimeter and two centre points, they authors found no clear correlation between optically measured obstruction maps and transmission factors derived from the wind field observations, but reported that the direction of the longest slope dictated the direction of local cold-air drainage flows, and hence that of the wind field. In their study, the sub-canopy flow was relatively uniform in spite of obvious heterogeneity in understorey density, height, and composition. However, their network observations yielded only quasi-simultaneous observations of carbon dioxide concentrations at the various locations through a manifold sampling system attached to a single infrared gas analyser, and did not include simultaneous observations of air temperature. In addition, network observations have been limited to domains of relatively small spatial extent and low density [25 m, 3 stations in Wilson and Meyers (2001); 50 m, 4 and 3 stations in Aubinet et al. (2003); Feigenwinter et al. (2004); 80 m, 7 stations in Staebler and Fitzjarrald (2004, 2005); 130 m, 3 stations in

Moderow et al. (2007)] with stations being located primarily around the outer boundaries of the sampling area, and not within the domain. In fact, the lack of knowledge of the space–time variability of scalar gradients in the canopy has been identified as one of the most likely causes hindering significant progress in the discussion of advective fluxes and the nighttime problem of underestimating carbon dioxide emissions from forested sites (Aubinet et al. 2010).

The plant canopy is part of the roughness sublayer (RSL), which is loosely defined as the part of the atmospheric boundary layer that is dynamically influenced by the length scales of the roughness elements in the canopy. It is assumed to extend from the mean height of the canopy crown to about three to five times the canopy height above ground (Garratt 1980, 1992; Raupach and Thom 1981; Thomas et al. 2006) depending on canopy density and other features of the canopy architecture (e.g. Novak et al. 2000; Poggi et al. 2004; Bohrer et al. 2009). The friction resulting from the interaction between the mean flow and the roughness elements leads to a generally weaker flow within the RSL. Studies have shown that with sufficiently weak flows, unpredictable non-stationary mesoscale motions, such as gravity waves and meandering motions (e.g. Hanna 1986; Anfossi et al. 2005) become important and can lead to abrupt wind direction shifts often exceeding 90° (e.g. Mahrt 2008, 2009). Waves are generally more important when sub-canopy and canopy stratification is significant. These wind direction changes complicate the discussion of terms in the energy and mass balances as a function of wind direction (e.g. Heinesch et al. 2008) as the definition of a uniform wind direction even for short averaging intervals is often ill-posed. A combined analysis of observations from several sensor networks including canopy data revealed that the time scales occupied by these small-scale mesoscale motions span minutes to hours, and spatial scales range from tens of metres to several kilometres (Mahrt et al. 2009). These scales therefore fall within the range of averaging periods of 30 and 60 min and domain sizes of up to hundred metres typically chosen for an evaluation of the surface budgets in the literature. It is therefore likely that these small-scale mesoscale motions also contribute to the variability of the surface budget terms particularly in the sub-canopy. The sub-canopy is here defined as the clear bole space between the canopy crown and the surface ground including the understorey. In the sub-canopy weak-wind conditions, with an arbitrary definition of horizontal winds $\leq 2\,\mathrm{m\,s^{-1}}$, prevail and the air is often decoupled from air aloft for most of the diurnal period even in moderately dense canopies (Thomas and Foken 2007). The small-scale mesoscale motions will be arbitrarily hereafter referred to as submeso motions to differentiate them from motions normally termed mesoscale with horizontal scales exceeding several kilometres.

In this article, the analysis of spatial observations from a sensor network installed a large domain of 180 by 205 m with ten stations operated over a period of several months in the sub-canopy of a forest with a dense overstorey was directed toward the following objectives:

- Analyse the variability of the space–time structure of the sub-canopy wind and temperature fields, as well as the resulting horizontal advection of sensible heat.
- Evaluate the impact of sensor network geometry and method of analysis on the magnitude and variability of horizontal advective components.
- Improve the understanding of the physical processes underlying the variability such as microfronts.

Investigations were not extended to include the variability of vertical advection because of the inability to measure meaningful mean vertical motions with a single anemometer (Vickers and Mahrt 2006; Heinesch et al. 2007), or scalars other than air temperature. A comprehensive evaluation of spatial structure requires truly simultaneous and

cross-referenced measurements across the domain. The calibration of individual temperature sensors against a common reference is more straight-forward than for other scalars such as humidity or carbon dioxide and typically leads to satisfactory precision allowing for the calculation of meaningful horizontal gradients.

2 Data Collection and Analysis

2.1 General Site Description

The dataset was collected in a 33 year-old mature Douglas-Fir forest located in the coast range of western Oregon, USA (AmeriFlux site US-Fir, 44.646° N latitude, 123.551° W longitude, 310 m elevation; see Fig. 1; Thomas et al. 2008) during the period from 28 Aug (DOY 241) through 17 Dec (DOY 352) 2008. The average canopy height is 26 m. The vertical structure of the vegetation canopy consists of a sparse understorey composed mainly of Salal (Gaultheria shallon) with a plant height of up to 0.8 m above ground level (a.g.l.) and the main tree crown space extending from 15 to 26 m a.g.l. separated by a clear bole space. The canopy is dense with a plant area index (PAI) of 9.4 $m^2\ m^{-2}$ optically measured in 2004 (Model LAI2000, Licor, Lincoln, Nebraska, USA). The vertical structure of the canopy and the high PAI lead to a reversed static stability regime in the crown space and the sub-canopy. During the day, the crown space and the above-canopy air are commonly unstably stratified with the maximum potential temperature observed at approximately 20 m a.g.l. and a weakly stably stratified sub-canopy and bole space. During weak winds at night, the crown space and air above the canopy are mostly stably stratified while the sub-canopy is isothermal with a minimum potential temperature at its top at 20 m a.g.l.. An infrequent increase in wind speeds at night leads to a vanishing potential temperature gradient from the surface ground to the top of the tower at 39 m a.g.l. The site is surrounded by moderately complex terrain with a flat saddle located to the northeast of the tower at a distance of approximately 600 m (Fig. 1).

2.2 Sensor Network

The sensor network consisted of ten stations each comprised of one two-dimensional (2-D) sonic anemometer (Model WAS425A, Vaisala Inc., Helsinki, Finland) and one air temperature sensor (external thermistor, Model HOBO H8 Pro, Onset Computer, Bourne, Massachusetts, USA) in a naturally ventilated radiation shield (model M-RSA, Onset Computer, Bourne, Massachusetts, USA) mounted at 1 m a.g.l. on a guyed tripod. Running 10 s averages of the raw measurements of wind speed and direction internally sampled at 1 Hz were interrogated and stored by a single data logger (Model CR5000, Campbell Scientific Inc., Logan, Utah, USA) using the serial digital interface (SDI) for the entire network. Wind data were subsequently aggregated into 1-min block-averages after transformation into a Cartesian coordinate system of horizontal vector components (u, v). No coordinate rotation was performed. Prior to field deployment, all 2-D sonic anemometers were cross-referenced against the horizontal wind speed of a single three-dimensional sonic anemometer (Model CSAT3, Campbell Scientific Inc., Logan, Utah, USA) in a wind tunnel over the range of 0.2 to 5.0 $m\,s^{-1}$ yielding a high precision much smaller than the resolution of the SDI output of 0.1 $m\,s^{-1}$. Measurements of air temperature (T) were collected and stored every 2 min by the onboard data logger of each sensor. Although shorter sampling intervals can be chosen, the large time constant of

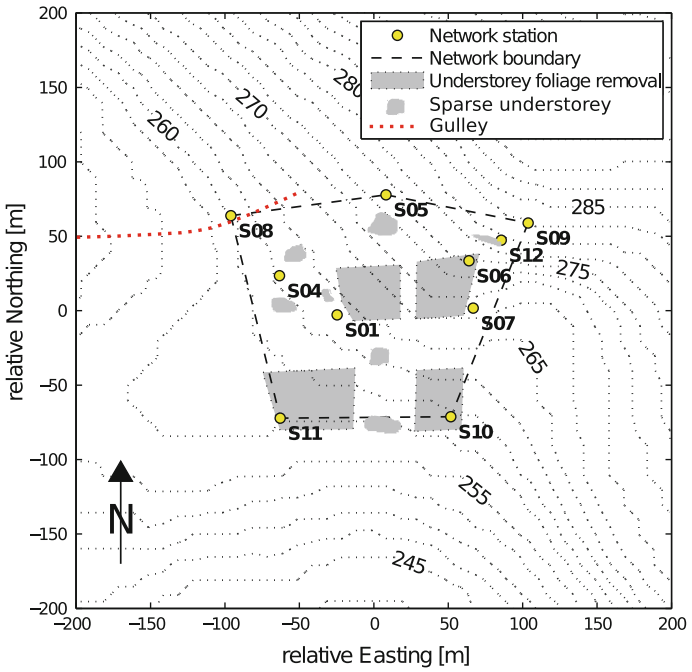

Fig. 1 Topographic map of the sampling domain and its surrounding with elevational isolines spaced at 2.5 m based on a digital elevation model with 10 × 10 × 0.3 m resolution (*Source*: Bureau of Land Management Oregon State Office; Publication Date: 31 July 1998; Title: "10 Meter Digital Elevation Model Collection Oregon, merged into 1 degree buffered blocks"). Also shown is the heterogeneity of the understorey: *grey shades* are areas where the understorey was defoliated with a chemical agent as part of a forest management experiment independent of and several years prior to this study; *grey*, *irregularly shaped areas* indicate a smaller understorey density due to natural variation. The overstorey is comprised of a very dense and homogeneous Douglas-Fir canopy with a plant area index of 9.4 m^2 m^{-2} and a high percentage of canopy closure

the thermistor ($\tau_{thermistor} = 122 \pm 6$ s, Whiteman et al. 2000) low-pass filters the signals that allows the computation of independent samples only every 4-min ($\approx 2\tau_{thermistor}$). During post-processing the recorded 2-min temperature records were linearly interpolated to 1-min resolution for the sake of synchronization with the wind data. However, results were analysed only for time scales $\geq$4 min (see Sect. 2.4) because of the inherent physical averaging of the signal. All thermistors were calibrated against one reference high-precision platinum resistance probe (Pt-100, Model RTD-810-3-36 with linearizer OM5-IP4-100-C, Omega Engineering Inc., Stamford, Connecticut, USA) prior to field deployment by simultaneously measuring the body temperature of a large aluminum block immersed in a temperature-controlled water bath over the range of 0 to 55° C. The precision (root-mean-square error, r.m.s. error) of the thermistor readings after applying sensor-specific linear correction functions was 0.10 K. Additional in-situ testing of the temperature sensors was performed at each station to estimate the radiative heating and cooling error in the naturally ventilated radiation shields (Anderson and Baumgartner 1998; Nakamura and Mahrt 2005; Mauder et al. 2008). For this purpose, temperature measurements from a well-calibrated platinum resistance probe (T_{ref}, Pt-1000, Model 41342, RM Young Company, Traverse City, Michigan, USA) in an aspirated radiation shield (Model 43408, RM Young Company, Traverse City, Michigan, USA) and

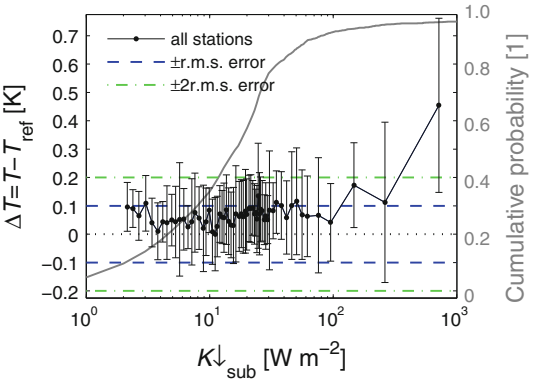

Fig. 2 Estimation of the daytime ensemble radiative heating error (ΔT) as the difference between the temperature measurements in the naturally ventilated radiation shields (T) and parallel temperature measurements in an aspirated radiation shield (T_{ref}) as a function of downwelling solar radiation in the sub-canopy ($K\downarrow_{sub}$) under clear sky conditions. Also shown is the standard deviation of each bin (*error bars*), the precision of the thermistors (root-mean-square error (r.m.s. error), *blue and green dashed lines*) determined in the laboratory experiments, and the cumulative probability density function of the sub-canopy solar radiation (*grey line*). For the majority of observations, the radiative heating error is negligible for the calculation of spatial temperature gradients as solar radiation levels are typically $\leq 100\,\mathrm{W\,m^{-2}}$

measurements of downwelling solar radiation in the sub-canopy ($K\downarrow_{sub}$, Model PSP, The Eppley Laboratory Inc., Newport, Rhode Island, USA) were taken in close proximity to each station for a period of 48 h under clear sky conditions in early July when solar irradiance and thus the error were expected to be maximal. Results showed that the ensemble temperature error $\Delta T = T - T_{ref}$ was smaller equal the determined r.m.s. error of the thermistors for most periods as solar irradiance were generally small ($\leq 100\,\mathrm{W\,m^{-2}}$) due to the closed and dense overstorey (Fig. 2). The high percentage of canopy closure also prevented significant radiative cooling errors at night. The experimentally determined error agreed well with model estimates for the same temperature sensor (see Fig. 2 in Mauder et al. 2008).

2.3 Sampling Domain and Station Placement

The ten network stations were arranged in a domain extending 180 m (west–east) by 205 m (north–south) (Figs. 1, 3). The maximum elevational difference across the sampling domain was approximately 25 m between station S09 and S11. The terrain dropped sharply across the transect of stations S09–S12–S06 in the north-east corner of the domain, and then continued to slope at moderate angles toward the outer stations S08, S11, and S10. Station S08 was placed in a shallow gulley. Independent of this study, the foliage of the understorey had been removed in some areas within the sampling domain several years prior to the observations presented here (Fig. 1), while the skeleton of the Salal bushes was left standing. The placement of the individual stations was motivated to include the full heterogeneity in local terrain, and understorey density and height to provide a framework for the evaluation of spatial and temporal variability of the wind and temperature fields. The station placement and domain size was also chosen based on the results from two preceding sensor networks with much smaller domains and less stations (first network: domain size 40 by 15 m consisting of six stations, *unpublished*; second network: domain size 110 by 70 m consisting of seven stations, see Mahrt et al. 2009).

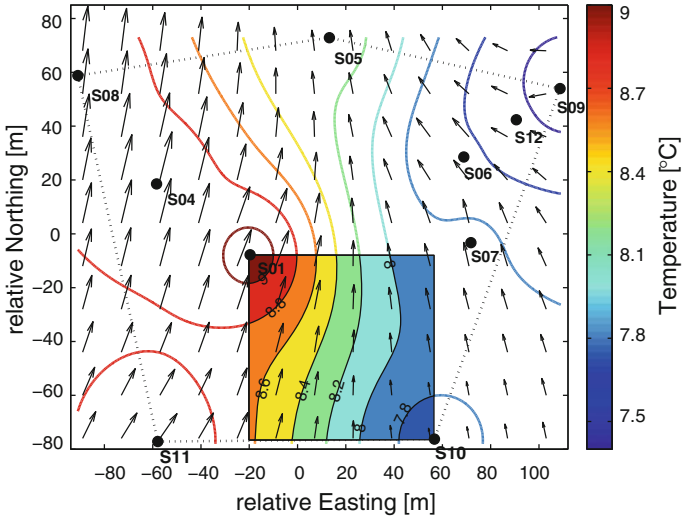

Fig. 3 Configuration of the sensor network consisting of ten stations within a sampling domain (*dotted lines*). Also shown is the average (64 min mode) structure of the air temperature (isolines) and the wind field (vectors) at 1 m above ground level over the period 23 September 2008 0100–0204. For estimation of the scale of wind speeds, the wind speed was 0.41 m s^{-1} in the *upper left corner* of the domain. Spatially discrete sampled winds and air temperatures were interpolated using the inverse square weighting method. The *filled rectangle* represents an example of the subdomain of the station pair S01–S10 when determining the variability of spatial gradients and horizontal advection (for details see Sect. 2.6). Spacing of temperature isolines was chosen as twice the r.m.s. error of the temperature sensors (see Sect. 2.2)

2.4 Multiresolution Decomposition

Data from all sensors were orthogonally decomposed into the local multiresolution basis set (e.g. Howell and Mahrt 1997) which decomposes a signal into unweighted averages over subrecords of dyadic width (2^n). The multiresolution decomposition technique was found suitable for the analysis of submeso motions that are generally of local and non-periodic character (e.g. Mahrt 2008; Mahrt et al. 2009). This simplest possible wavelet basis set offers several advantages over other commonly applied spectral decomposition techniques such as the fast Fourier transform (FFT) as it does not assume any periodicity of the signal, the spectral peak corresponds to the dominant local event, it satisfies Reynolds averaging independently at all scales, and it has a finer resolution for smaller averaging lengths compared to the global FFT. Data were divided into 64-min sub-records each consisting of $N = 2^M = 64$ data points of the 1-min averages. $M = 6$ is the number of multiresolution modes for each sub-record with 2^{M-m} different averaging windows of 2^m data points, and $m = 0, \ldots, M$. The corresponding multiresolution time scales are $2^{M-m} = 64, 32, 16, 8, 4, 2, 1$ min. An arbitrary signal ϕ can be written as the sum of M multiresolution modes for the pth sub-record such that

$$\overline{\phi}(p) = \frac{1}{M} \sum_{1}^{M} \phi_m(p). \tag{1}$$

From this follows that the average associated with the $m = M$ mode is the sub-record mean, while $m = 0$ corresponds to the original signal. The construction of 64-min sub-records required subsequent intervals to overlap by 4-min in order to start each sub-record at the full

hour, which did not lead to any detectable contamination of the statistics of the entire dataset. The total number of 64-min sub-records was $P = 1765$ (night: 925, transition period: 157, daytime: 683).

2.5 Bulk Measures of Network Statistics

As a first step, a stochastic analysis of the network data was performed using various measures of time and space variability applied separately to each multiresolution time scale (see Sect. 2.4) averaged over the entire dataset. The reader is referred to Mahrt et al. (2009) for a more complete definition and discussion of these measures, while only a brief overview will be given here for completeness. The equations below are defined for any variable $\phi = u, v, T$ between the two stations i and j separated by distance r_{ij}. Note that the indices for sub-record number $p = 1, \ldots, P$ and multiresolution mode $m = 1, \ldots, M$ will be omitted in the following equations for clarity of presentation. The number of paired stations ij for the network configuration was $10![2!(10-2)!]^{-1} = 45$.

Spatial variability of the flow: was computed for each station i as its deviation from the 1-min spatial network average denoted by $\langle\ \rangle$,

$$\tilde{\phi}_i = \phi_i - \langle\phi\rangle. \tag{2}$$

The wind components were then combined into the velocity scale $V_{Domain,i}$ defined as

$$V_{Domain,i} \equiv \overline{\sqrt{\tilde{u}_i^2 + \tilde{v}_i^2}}, \tag{3}$$

where the overbar implies a temporal average over the 64-min record or the entire experiment.

Two-point correlation coefficient: is defined as the spatial correlation coefficient

$$R_{\phi,ij}(r_{ij}) = \frac{\overline{\phi_i' \phi_j'}}{\sigma_{\phi_i}\sigma_{\phi_j}}, \tag{4}$$

where the primes denote the deviation from the temporal average over the experiment's duration for each station. In case of the wind data, the two horizontal components were combined into $R_{uv}(r_{i,j}) \equiv \sqrt{(R_u^2 + R_v^2)/2}$.

Two-point structure function: this dimensional second-order measure was calculated between two stations using the expression

$$S_{\phi,ij}(r_{ij}) = \frac{1}{P}\sum(\phi_i - \phi_j)^2. \tag{5}$$

The structure functions of the wind components combined into $S_{uv}(r_{ij}) \equiv \sqrt{S_u^2 + S_v^2}$.

2.6 Bulk Measures of Variability in Gradients and Horizontal Advection

We also examined the space–time variability of temperature gradients and horizontal advection using the measures defined below. The computation of gradients and advective components requires the data to have physically meaningful values and therefore required a reconstruction of the decomposed signals. Since the multiresolution decomposition at mode m contains only the perturbations from the average at mode $(m-1)$, physical values of

wind components and temperatures for all modes $0 < m \leq M$ were constructed by summing over the $0, \ldots, m$ multiresolution modes for each sub-record. The sampled variable fields $u_m(x, y)$, $v_m(x, y)$, $T_m(x, y)$ containing all stations were then non-linearly interpolated using the inverse square weighting method to a resolution of 0.5 m in both longitudinal (y) and latitudinal (x) directions, with the recognition that only motions on horizontal scales significantly greater than the minimum station spacing were resolved, as it takes a minimum of several stations to resolve individual motions. The horizontal temperature gradients between two original stations indexed by i and j separated at distance $r_{i,j}$ for each sub-record were calculated as

$$\Gamma_{x,ij}(r_{i,j}) = \frac{\langle \partial T_{ij} \rangle}{\partial x}, \tag{6}$$

and

$$\Gamma_{y,ij}(r_{i,j}) = \frac{\langle \partial T_{ij} \rangle}{\partial y} \tag{7}$$

by fitting a plane to the interpolated values of the subdomain defined by the stations' locations (see the filled rectangle in Fig. 3 for an example of the station pair S01–S10); the angle brackets imply spatial averaging over the subdomain. The temporal average $TAG_{ij}(r_{i,j})$ and time-dependent variance $TVG_{ij}(r_{i,j})$ of the spatial temperature gradients are given by the expressions

$$TAG_{ij}(r_{i,j}) = \overline{\Gamma_{ij}(r_{i,j})}, \tag{8}$$

$$TVG_{ij}(r_{i,j}) = \sqrt{\frac{1}{P-2} \sum \left(\Gamma_{ij}(r_{i,j}) - \overline{\Gamma_{ij}(r_{i,j})} \right)^2}, \tag{9}$$

where the overbar denotes temporal averaging over the entire dataset. Measures of the within-domain, time-independent variance of the temperature gradients SVG for each sub-record was computed using the equation

$$SVG = \sqrt{\frac{1}{P-2} \sum \left(\Gamma_{ij}(r_{i,j}) - \langle \Gamma \rangle \right)^2}, \tag{10}$$

with the operator $\langle\ \rangle$ implying spatial averaging over all 45 station pairs. In a last step, its temporal average $\overline{SVG}$ and time-dependent variability of spatial variance $\overline{SVG'^2}$ were computed over the entire dataset analogously to Eqs. 8, 9.

Measures of the variability of horizontal advection were computed similarly. The horizontal advection $\Psi_{ij}(r_{i,j})$ between two stations indexed i and j for each sub-record was computed by combing the spatial temperature gradients (Eqs. 6, 7) with the interpolated wind components averaged over the subdomain leading to

$$\Psi_{ij}(r_{i,j}) = \int \int \left\langle \left(u_{ij} \right| \Gamma_{x,ij}(r_{i,j}) + \langle v_{ij} \rangle \Gamma_{y,ij}(r_{i,j}) \right) dxdy. \tag{11}$$

The temporal average $TAA_{ij}(r_{i,j})$ and the time-dependent variance $TVA_{ij}(r_{i,j})$ of the horizontal advection were computed in a fashion analogous to those of the temperature gradients (Eqs. 8, 9).

As the computation of meaningful spatial temperature gradients and advection requires precise measurements of the between-station temperature differences ($\partial T_{i,j}$, see Eq. 6), a brief discussion of the measurement uncertainty propagating into the computation of $\Gamma_{i,j}$ and $\Psi_{i,j}$ is presented here. Observed between-station differences are assumed to be comprised of

$\partial T_{i,j} = \partial T_{\epsilon,instr} + \partial T_{system,instr} + \partial T_{real}$, where $\partial T_{\epsilon,instr}$ stands for the random instrumental error, $\partial T_{system,instr}$ for the systematic instrumental error, and ∂T_{real} for the true physical signal. The term $\partial T_{system,instr}$ can be neglected after application of the linear correction models derived from the laboratory calibrations, and $\partial T_{\epsilon,instr} =$ r.m.s. error $= 0.10$ K (see Sect. 2.2). In the majority of cases ($\geq$94%), $\partial T_{i,j} \geq \partial T_{\epsilon,instr}$ for the observed between-station temperature differences sampled every 2 min. Furthermore, the random instrumental error is expected to vanish when temporally averaging over the duration of the experiment in case of linear statistics. The measurement uncertainty, i.e., the precision of the sensors is therefore assumed to have a negligible impact on the observed statistics and advection patterns.

3 Results and Discussion

Results were generally partitioned into diurnal periods differentiating between night, transition period, and day based on geometrically calculated azimuth and zenith angles for the site. Transition period was defined as the 64-min sub-record in which sunrise or sunset occurred.

3.1 Wind and Temperature Fields

The presentation of the wind statistics will be followed by those of temperature before comparing the space–time structure of both variables. The deviation of the flow at each station in relation to the spatial (domain) average based on the 1-min data $V_{domain,i}$ (Eq. 3) showed differences in its diurnal behaviour, as well as modest systematic differences among stations (Fig. 4). One must recall that $V_{domain,i}$ is defined as a measure of the total spatial variability of the flow magnitude (scalar average) as the sign of the deviations and hence the differences in wind direction are not preserved in its mathematical definition. The spatial variability of the sub-canopy flow was generally larger during the day and its wide probability distribution indicated a large temporal variability compared to the very narrow peaked distribution at night. Station S08, which was located in a shallow vegetated gulley, was characterised by a modestly larger deviation from the spatial average than any other station in the network at night. Possible explanations include that it was subject to flows not captured by the rest of the domain, or caught in an oscillation between a flow aligned with the orientation of the gulley and the larger, domain-scale flow, as suggested by the two-peaked distribution of the wind directions at this station (not shown here), which was unlike any other station. The magnitude of $V_{domain,i}$ was at the lower boundary compared to other wind networks analysed by Mahrt et al. (2009, see their Table II) with a median of 0.20 and 0.13 m s^{-1} for day and night conditions respectively. The network data for the same site included in Mahrt et al. (2009) was observed in a smaller domain with a different network configuration and over a shorter period of time (see Sect. 2.3), which may have caused the discrepancies. In addition, computational differences may arise depending on whether the data are first spatially and subsequently temporally averaged (as in Mahrt et al. 2009), or in reversed order as applied here. The authors argued that the magnitude $V_{domain,i}$ may increase with domain size, as larger domains capture a greater variety of submeso-scale motions at a broader range of scales, and with complexity of the terrain. Note that the magnitude of individual 1-min deviations exceeded the precision and resolution of the wind sensor data and instrumental uncertainty could therefore be excluded to significantly impact the observed spatial variability of the wind. Overall, the small $V_{domain,i}$ found in this study indicates a very homogeneous wind field despite the observed differences and the complexity of the topography and

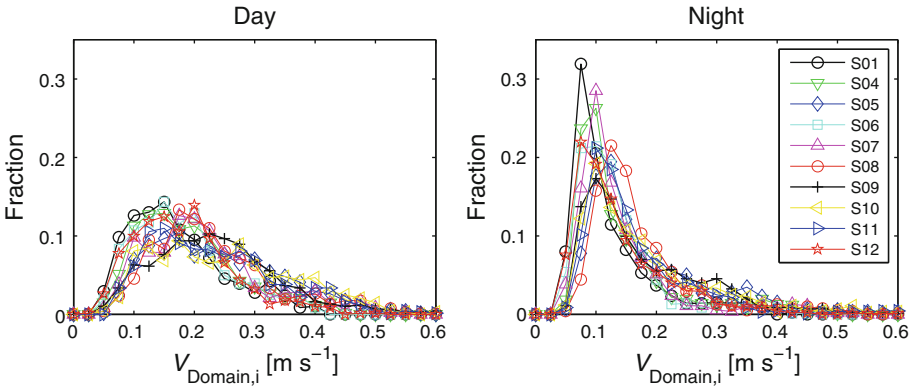

Fig. 4 Probability density function of the spatial variability of the flow magnitude ($V_{Domain,i}$, see Sect. 2.5) at the 1-min time scale for all network stations computed over the entire dataset

understorey. This finding is in direct agreement with results from Staebler and Fitzjarrald (2005), who found that the flow sampled around the outer perimeter of a smaller domain of 80 by 80 m showed only small deflections or attenuations despite significant variability of the understorey vegetation structure and terrain.

The two-point correlation of the flow $R_{uv,ij}$ was a function of separation distance between stations for all time scales (Fig. 5). The fast decay of $R_{uv,ij}$ with increasing separation distance, which was particularly visible for short time scales, demonstrates that these motions are short-lived and small in spatial extent. In contrast, larger-scale transient motions moving at high velocities would maintain a high spatial correlation at the shorter time scales. The variability of the correlation $R_{uv,ij}$ for a specific separation distance was largest for the longest time scale (the 64-min mode containing the time-averaged mean), which suggests that each station has a location-specific wind microclimate. This wind microclimate is likely to depend on the presence of individual flow obstacles such as bushes, tree boles, and local variation of the topography leading to systematic deviations as was demonstrated for the spatial variability of the flow magnitude ($V_{domain,i}$) at station S08. Note that the decorrelation of the 2- and 4-min wind modes were much less compared to that found by Staebler and Fitzjarrald (2004) for 3-min averaged sub-canopy winds. Their study reported a correlation coefficient of ≈0.15, while in this study the correlation remained stronger at ≈0.5 for similar scales of 100 to 120 m. One may speculate that the more complex terrain at our site generates motions that are of similar spatial scale than that of the topographic heterogeneity defined by the size of the shallow valley in which our site is located, which is on the scale of several hundred metres and thus larger than the sampling domain. One would therefore anticipate the spatial correlation to remain larger at our site when compared to the flat site of Staebler and Fitzjarrald (2004), which may lack the presence of topography-induced larger eddies.

The strong diurnal variations in the magnitude of the dimensional structure function of the flow $S_{uv,ij}$ (Fig. 6) were in agreement with the larger spatial variability $V_{domain,i}$ during daytime conditions observed before. The structure function is a measure of the absolute differences between stations (Eq. 5) rather than their spatial or temporal correlation. The diurnal differences in $S_{uv,ij}$ were on the order of a factor two to three. The structure function rapidly increased with increasing separation distance for smaller time scales, while the larger time scales appeared to be almost independent of the space scales captured by the domain. This indicates that short-lived motions (1, 2, 4 min) significantly contribute to the structure

function and are well resolved by the station spacing of the network, while the domain is possibly too small to resolve motions on longer time scales. An alternate explanation may be the absence of larger scale gradients and spatial differences in wind speed and direction that would require deep pressure perturbations on spatial scales far exceeding those of the sensor network as driving force.

The analysis of the space–time structure of the temperatures revealed some similarities, but also important differences compared to that of the velocities. The two-point temporal correlation of the temperature $R_{T,ij}$ behaved similarly to that of the velocity field with the exception of the largest 64-min mode, which showed no decorrelation even for the largest spatial scales (Fig. 5). This independence of spatial scale can be explained by the diurnal cycle of air temperature forced by the solar heating during the daylight hours and the radiative cooling at night. The almost perfect correlation independent of location indicates that all stations were consistently participating in this diurnal oscillation, while effects of systematic station-specific decoupling, e.g. through the presence of cold air pools, were negligible or absent at this site. In general, the temporal correlation of the temperature signal remained higher compared to that of the flow for all time scales (multiresolution modes) and identical spatial scales (separation distances). The increased scatter in correlation of temperature signals detected for the shortest scales (4 min) at night was caused by data collected at station S01. This suggests that temperature observations at this station were often decoupled from the temporal thermodynamics of the rest of the domain. A possible explanation may be its close proximity to a somewhat taller group of Salal bushes in the understorey, which may have led to systematically higher nighttime temperatures (see e.g. Fig. 3) because of the mechanical sheltering and radiative transfer from the vegetation. A two-point correlation analysis of the observed radiative heating error (ΔT, see Sect. 2.2) did not yield any systematic behaviour with spatial or temporal scale and showed a generally low correlation ($R_{\Delta T,ij} \leq 0.3$) across the entire domain (not shown here), and can therefore be excluded as an important source of uncertainty.

Despite the similarity in the magnitude of the diurnal differences of the dimensional structure function of the wind and temperature fields, important differences were found for $S_{T,ij}$ emphasizing the contrasts between the signals (Fig. 6): motions on the longest time scales showed the strongest dependence on spatial scale, whereas the structure function for small motions was almost constant and seemingly independent of separation distance. Obviously, motions on short time scales were insufficiently resolved by the configuration of the network even in the densest part of the domain with a minimum separation distance of 21.5 m between stations S09 and S12, while motions on longer time scales were well captured. The former result is in agreement with the interpretation of the correlation analysis and verified the small-scale nature of the motions transporting heat. The variability of the structure function was greater for a specific separation distance during the day than at night, which confirmed the pattern of diurnal dependence of space and time variability on light regime for this site.

3.1.1 Conceptual Space–Time Variability Diagram

The results from the stochastic analysis of the sub-canopy wind and temperature fields can be conceptualised in a diagram constructed from axes representing the space and time domains (Fig. 7). The analysis yielded that the motions predominantly contributing to the variability of the wind and temperature fields occupy similar space, but different time scales (see shapes with text in boldface in Fig. 7). We recall that the variability of the flow in space and time was dominated by small-scale and short-lived motions, and that it was adequately resolved by the network geometry, i.e., stations spacing and domain size. However, the longest motions

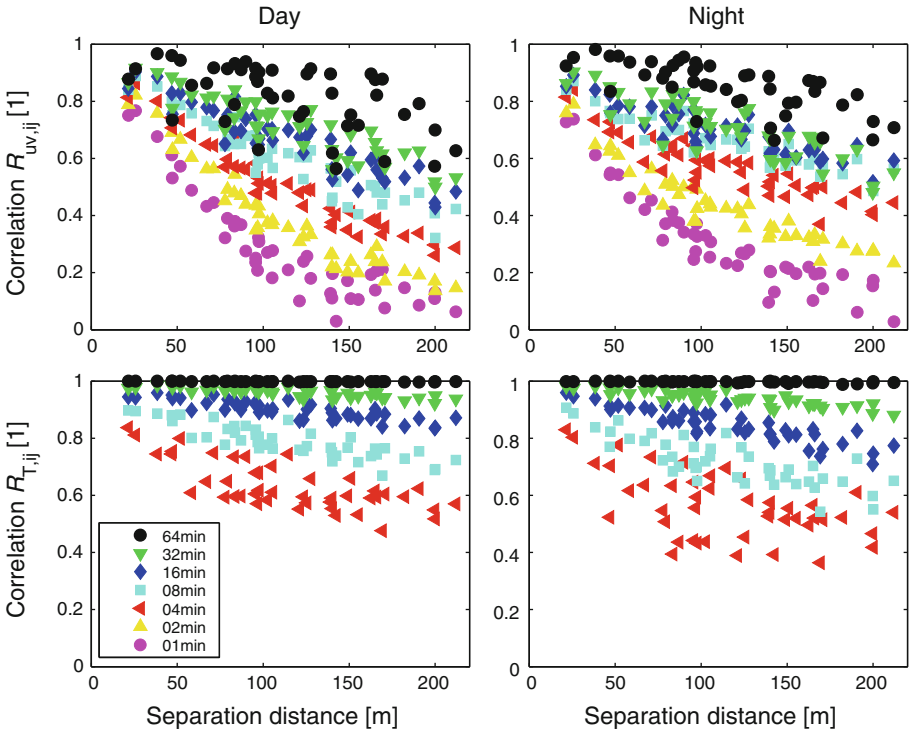

Fig. 5 Two-point correlation of the wind ($R_{uv,ij}$, see Sect. 2.5) and temperature ($R_{T,ij}$) versus separation distance between stations as a function of time scale (multi-resolution mode, see Sect. 2.4) for all 45 station pairs over the entire dataset

defining a station's wind microclimate contribute a rather stationary signal to the wind statistics at a station that is of secondary importance to the total variability and is restricted to the smallest spatial, but largest temporal scales resolved in this study. In contrast, the diurnal course of temperature driven by the surface radiative transfer is the main determinant of temporal variability of the air temperature, whereas it contributes little to its spatial variability as demonstrated by the almost perfect correlation of the temperature signal independent of separation distance. Particularly during the daylight hours, the spatial variability of the temperature field is dominated by scales smaller than those resolved by the network. These significant differences in the space–time variability of the sub-canopy wind and temperature fields may cause a mutual incompatibility of the signals and thus be an important source for the variability of the resultant horizontal advection of sensible heat discussed in the subsequent section. Furthermore, the scale mismatch renders Taylor's hypothesis invalid for the observed sub-canopy flow, as there is no unique, simple symmetry between temporal and spatial temperature gradients given by the mean domain-averaged flow (diagonal line in Fig. 7).

Despite the obvious contrasts in space–time structure between the flow and temperature, both variables were subject to influences of the immediate surround of a station, here termed the local field. The local field is defined by the variations of understorey density and architecture, and local terrain such as gullies and slopes on a submetre to metre scale. In other words, the placement of a station within a network can have a significant impact on the spatial and temporal variability observed at that location.

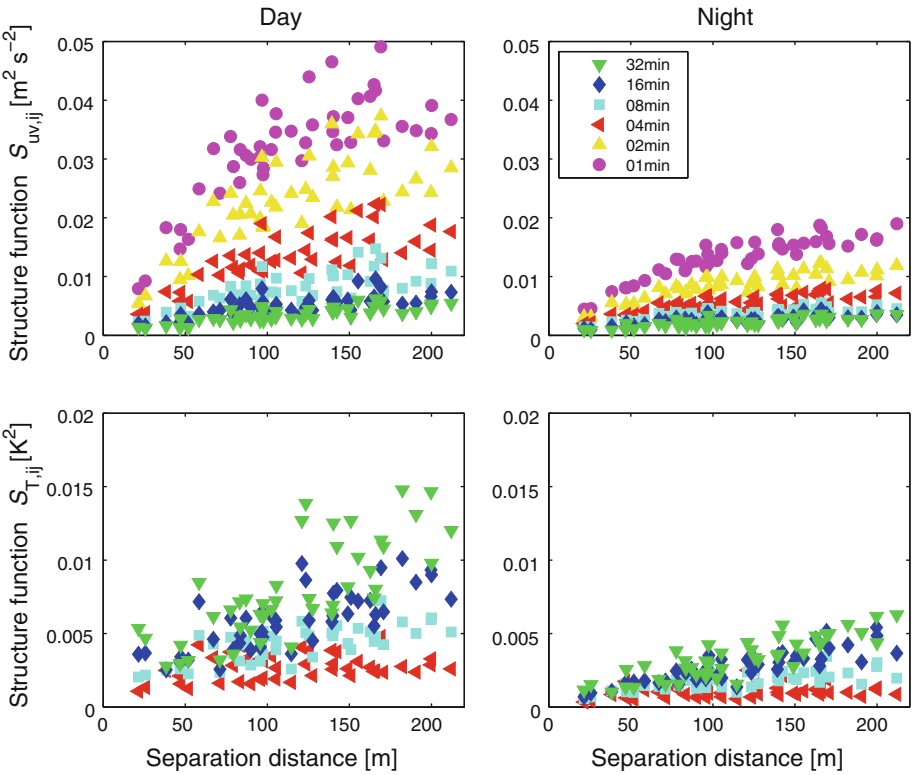

Fig. 6 Same as Fig. 5 but displaying the two-point structure function of the wind ($S_{uv,ij}$, see Sect. 2.5) and temperature ($S_{T,ij}$)

3.1.2 Causes of the Observed Variability

In an attempt to provide some explanation for the motions dominating the observed time and space variability an analysis of microfronts in the wind field was performed. Microfronts are only one possible mode of submeso motions contributing to the variability, but their analysis is straight-forward compared to more complex modes such as linear canopy waves, non-linear turbulence-wave interactions, and local circulations including gravity-driven cold-air drainage. Note that the microfronts of interest here are different from those that have been studied in connection with the shear-induced sweep-ejection cycle in tall canopies. In the literature, there is sufficient experimental evidence that the time scales of sweep-ejection motions are typically smaller ($\leq$1 min) than those of the submeso motions analysed here. Microfronts were defined as the most extreme 5% of the probability density function of the temporal differences between adjacent windows of identical length shifted over the time series of 1-min averaged winds at 1-min increments at each station. The window length was varied between 4, 8, 16, 32, and 64 min. After detecting the microfronts for each station, their coherence was determined by counting the number of stations participating in a specific event for all detected incidents. One shortcoming of the detection scheme is its dependence on the magnitude of the temporal differences: it is conceivable that a slow-moving microfront engulfing the entire domain will not be detected at all stations because of the location-specific

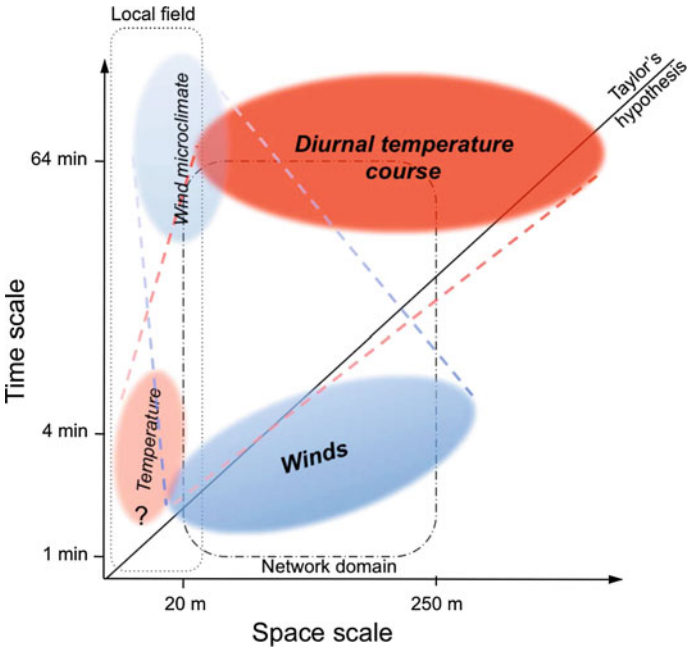

Fig. 7 Conceptual diagram showing the areas occupied by the sub-canopy wind (*blue*) and temperature (*red*) fields in the space and time domains. Shapes are shown for the shortest (1 and 4 min) and longest (64 min) motions analysed in this study, which are connected by the *dashed blue* and *red lines* indicating motions on intermediate scales. The dominant contribution is identified in *bold typeface*. The slope of the line 'Taylor's hypothesis' (*solid thick*) is equal to the inverse domain-averaged horizontal wind speed (day: 0.25 m s^{-1}, transition period 0.22 m s^{-1}, night: 0.18 m s^{-1}). Also shown are the boundaries captured by the sensor network in this study (*black dash-dotted line*) and the local field (*black dotted line*). The definition of the local field is proposed here as the immediate surround of a sensor where individual elements such as bushes, tree boles, and variations of the terrain such as gullies and slopes affect the wind and temperature field

differences in the magnitude of the change particularly for short window lengths. However, the method should be robust for the strongest microfronts, hence the selection of the most extreme 5% of the probability density function.

The outer stations S05, S10, and S11 were found to be the most unique sampling locations showing the most microfronts detected at a single station only. We recall that stations S10 and S11 were located in the lowest part of the domain and at the outer perimeter of the areas where the understorey was defoliated (see Fig. 1). In contrast, the coherence of microfronts defined as an event when exactly nine out of the ten stations are participating in an event was smallest for station S07. The reasons for this anomalous behaviour remain unknown as obvious local variations of the understorey or terrain were absent at this station. In general, the spatial patterns in the microfront analysis showed little variability with varying detection window length, and are therefore considered to be robust. In summary, patterns in the spatial coherence of microfronts confirmed the importance of a station's local field. The agreement between results from the microfront analysis and the stochastic bulk measures indicates that the microfront may be an important mode of submeso motions contributing to the sub-canopy variability of the wind fields. The release of machine-generated fog to visualise the sub-canopy flow at the site qualitatively confirmed that microfronts commonly propagate through the network and maintain a high spatial coherence.

3.2 Temperature Gradients and Horizontal Advection

First, spatial temperature gradients will be discussed followed by a presentation of the resultant horizontal advection. Note that the analysis of temperature gradients was based on the spatially interpolated temperature fields constructed from the point-measurements at all ten stations using the inverse square weighting method (see Sect. 2.6).

The spatial temperature gradients were more systematic at night than during the day, and decreased with increasing station spacing (Fig. 8). This result is in agreement with the findings of the higher daytime variability of the bulk stochastic measures in the previous section. At night, the time-averaged gradients TAG_{ij} were found to become constant and thus independent of spatial scale only for separation distances exceeding 100 to 150 m. During the day, gradients showed large scatter with frequent changes in sign and only a weak dependence on spatial scale. Contrary to the nighttime case, daytime gradients did not converge to a constant value even for the largest spatial scales of the domain. The time-averaged gradients showed little variability with temporal scale (multiresolution mode), but varied strongly with spatial scale and location with the domain (separation distance and position of paired stations). The time-dependent variability of the spatial temperature gradients TVG_{ij} decayed with increasing station spacing in a non-linear fashion, which suggests that a larger domain captures more stationary motions leading to a reduction of temporal variability (Fig. 8). It remains a speculation if TVG_{ij} would increase for larger spatial scales greatly exceeding those of the current domain by capturing different and more heterogeneity in other parts of a complex landscape.

One of the study's objectives was to evaluate the impact of the network configuration on the spatial gradients and advection estimates. Therefore, the computation of spatial gradients was repeated based on a subset of stations including observations from the outer stations only (S08, S05, S09, S10, S11, see Figs. 1, 3). This configuration allowed for testing the common assumption of linear gradients within a domain (e.g. Moderow et al. 2007). In general, the temporal averages and the variability of the temperature gradients computed from this subset exceeded those derived from the full domain indicating that at least for this site, it is insufficient to approximate spatial gradients linearly (see open symbols in Fig. 8). Another test aimed at the evaluation of alternate spatial interpolation algorithms. Changing the interpolation algorithm from the inverse square weighting to the cubic spline method resulted in significantly larger scatter of the temporal variability of the spatial temperature gradients and its increase toward larger spatial scales (not shown here). Both tests demonstrated that the computed spatial temperature gradients, and hence the horizontal advection, are sensitive to the number and placement of the stations, as well as to the interpolation method.

Consistent with the temporal variability of the spatial gradients, the within-domain, time-independent variability of the temperature gradients (SVG, Eq. 10) decreased with increasing time scale in both its temporal average ($\overline{SVG}$) and variance ($\overline{SVG'^2}$) (Fig. 9). Daytime values were much larger than those observed during the transition periods or at night, which agreed with the larger variability observed in the time domain. This observation for the sub-canopy temperature field agrees with that of the variability of the spatial carbon dioxide concentration gradients in the trunk space of a tall canopy, which peaked during the day (Heinesch et al. 2007). The authors attributed their finding to a larger sensitivity to local source heterogeneity, which implies an enhanced transport of the scalar signal by an increased efficiency over larger distances. However, based on the stochastic analysis of the space–time structure of the temperature field presented here, the local source heterogeneity of the scalar signal itself may be larger during the day leading to the observed elevated daytime variability.

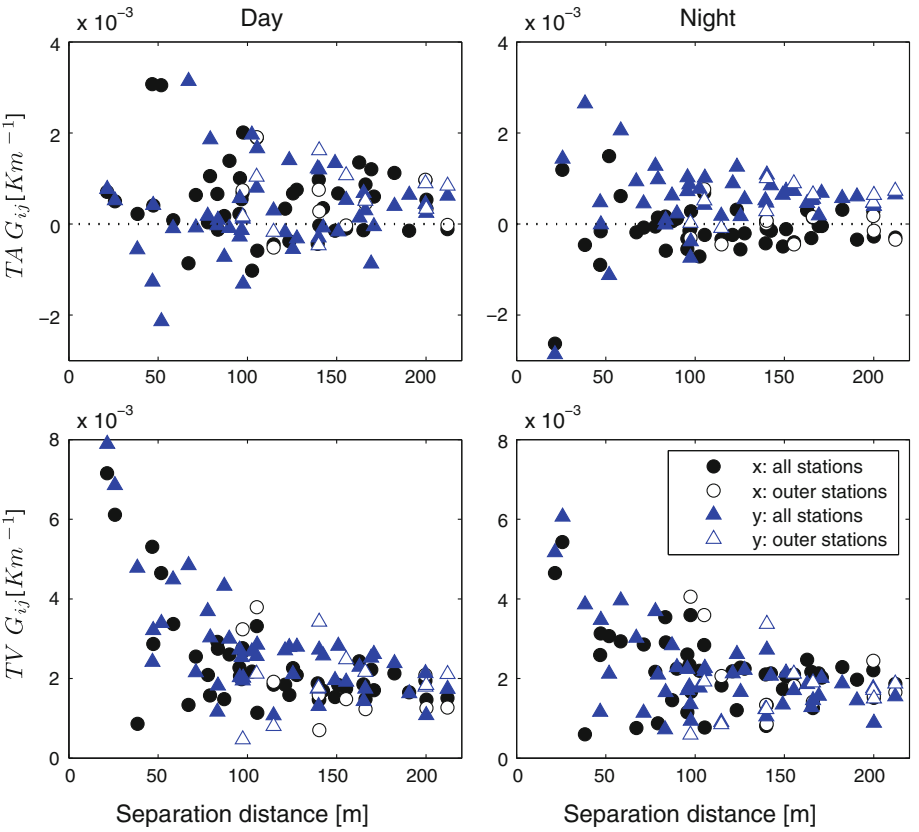

Fig. 8 Time average (TAG_{ij}, Eq. 8) and time-dependent variability (TVG_{ij}, Eq. 9) of spatial temperature gradients for the 32-min time scale (multiresolution mode) as a function of station spacing over the entire length of the dataset for the longitudinal (y) and latitudinal (x) directions. Measures were evaluated for two different network configurations (see Fig. 3): all ten stations (S01–S12, *filled symbols*), and outer stations only (S08, S05, S09, S10, S11, *open symbols*)

Note that the mean transport velocity, i.e., the mean horizontal wind speed, averaged over the experiment duration showed little differences with daylight regime (day: $0.25\,\mathrm{m\,s^{-1}}$, transition period $0.22\,\mathrm{m\,s^{-1}}$, night: $0.18\,\mathrm{m\,s^{-1}}$), but absolute between-station differences were by a factor of two larger during the day compared to the night case as demonstrated by the increased structure function of the wind (Fig. 6). Hence, the increased spatial variability of daytime scalar gradients may be caused by a combination of increased scalar source heterogeneity and an increased variability of the local transport.

In contrast to the temporal variability of spatial temperature gradients, the variability of the time-averaged horizontal advection of sensible heat, TAA_{ij} (Eq. 11), was smallest for the smallest spatial scales, then increased until approximately the 100 m scale, and remained large for all scales beyond (Fig. 10). This finding suggests that the small-scale pockets of air characterised by large variations in temperature on scales smaller than the resolution of the network (see Sect. 3.1) contribute little to the advective flux on scales $\leq$100 m, likely due to the fundamentally different spatial and temporal scales of the flow transporting the sensible heat (see Fig. 7). However, a clear distinction between the effect of the spatial variability

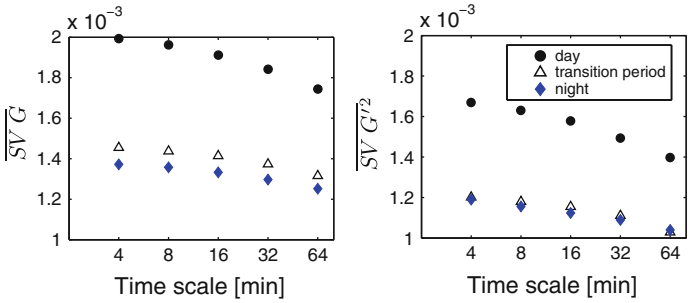

Fig. 9 Temporal average ($\overline{SVG}$) and time-dependent variability of the spatial variance ($\overline{SVG'^2}$, see Eq. 10) of spatial temperature gradients as a function of time scale (multi-resolution mode) over the entire length of the dataset

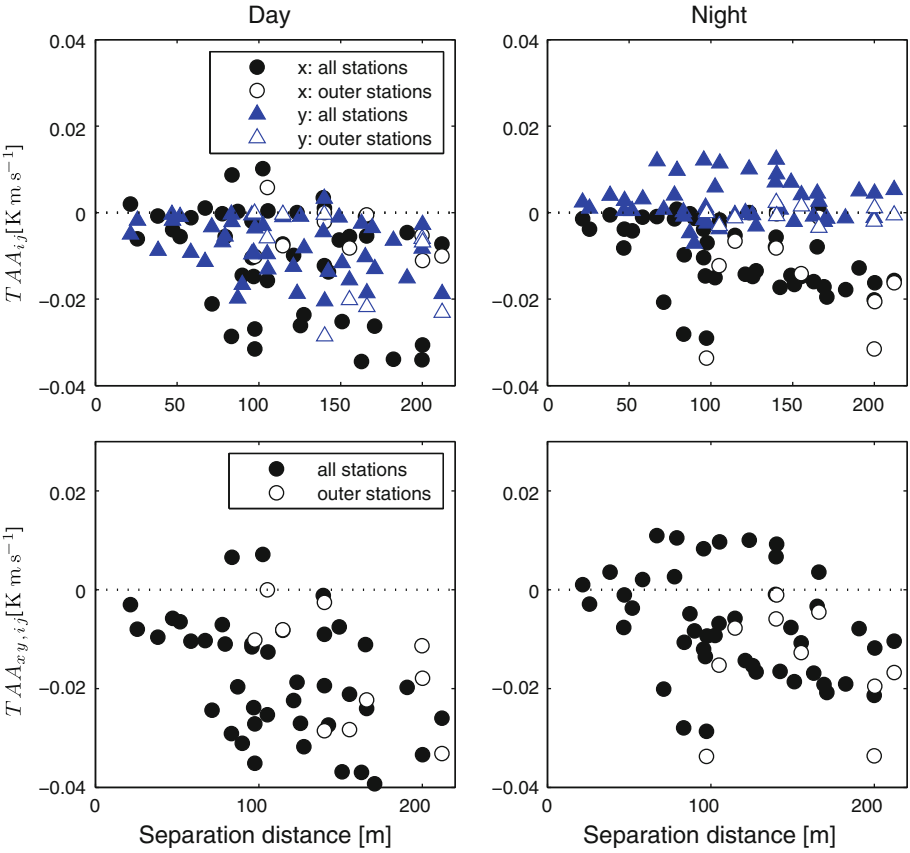

Fig. 10 Direction-wise ($TAA_{x,ij}$, $TAA_{y,ij}$, *top*) and total resultant ($TAA_{xy,ij}$, *bottom*) temporal average of the horizontal advection of sensible heat for the 32 min mode as a function of station separation distance (see Sect. 2.6). Measures were evaluated for two different configurations: all ten stations (S01–S12), and outer stations only (S08, S05, S09, S10, S11)

between the wind and temperature field on the resultant horizontal advection is difficult, as the dominating motions occupy similar spatial scales. The variability of the advective fluxes with spatial scale was similar for daytime and nighttime data, while the daytime estimates showed a more consistent, negative sign over the duration of the experiment. Generally, the smallest spatial scales yielded horizontal advective fluxes approximately equal to zero, while larger spatial scales showed an increase in magnitude. The time-averaged horizontal advection of sensible heat $TAA_{xy,ij}$ was found to be of consistent sign only for spatial scales exceeding 180 m, which is close to the upper limit of scales resolved by the network. Based on these findings, the recommended horizontal dimension of the control volume used for an evaluation of the contribution of all components of the surface energy balance must be $\geq$180 m to yield the most consistent results, at least for this site. However, a larger sampling domain may yield a larger recommended control volume as an increased domain size is likely to include more spatial heterogeneity, or heterogeneity of a larger spatial scale. Without direct measurements, no assumption of the behaviour of the heterogeneity with spatial scale can be made as no scales larger than that of the sampling domain can be inferred. In a case when heterogeneity scales with spatial extent, the selection of an optimal size may prove difficult. The method described by Staebler and Fitzjarrald (2004) to estimate an appropriate sampling domain size is conceptually different from that proposed here, as our method is based on the combined evaluation of the temperature and wind fields, and not solely on that of the coherency of the flow. Note that the sign of nocturnal horizontal advection changed frequently within 50 to 150 m of scale, which has been a common size for control volume of advection studies in the literature. This finding may provide an explanation for the inconsistent, ambiguous results reported for the contribution of advective components at various sites, which ultimately have left the problem of the most suitable experimental design for an evaluation of the energy and mass balances in canopies unsolved (e.g. Aubinet et al. 2010). Particularly at night, the magnitude of the horizontal advection of sensible heat was larger when evaluated from the reduced network size constructed from the outer stations only, which is in agreement with the larger spatial gradients observed for this test configuration. This finding again emphasizes the importance of within-domain observations to estimate local the wind field and the non-linear temperature gradients adequately.

4 Conclusions

This study examined the space–time variability of the wind and temperature field, spatial temperature gradients, and the resultant horizontal advection of sensible heat in the sub-canopy of a dense coniferous forest calculated from network observations at ten stations over several months. One arrives at the following conclusions with regard to the three objectives of this study:

- Fundamental differences were found in the space–time structure of the motions dominating the variability of the sub-canopy wind and temperature fields, which can be used to construct a conceptual space–time diagram of the variability (Fig. 7). The dominating motions have similar space, but different time scales. This scale mismatch renders Taylor's hypothesis invalid for the sub-canopy flow and substantially aggravates the computation of the meaningful horizontal advection estimates without dense spatial observation.
- The strongly non-linear nature of the spatial sub-canopy temperature gradients requires an adequate resolution of the temperature field by including observations within the sampling domain in addition to measurements around its perimeter. The non-linearity of gradients

may provide an explanation for the ambiguous results on the contribution of horizontal advection to the canopy budgets of energy and mass reported in the literature. A larger number of stations facilitates a better resolution of the non-linear spatial gradients of the wind and temperature fields, while no quantitative recommendation can be made for an optimal number of stations based on the existing data.

– The recommended domain size of the control volume exceeds selections commonly used in energy and mass balance studies and is on the order of hundreds of metres (≈180 m at the study site), but likely to be site dependent. A larger sampling domain may yield a larger recommended control volume as an increased domain size could include more spatial heterogeneity, or heterogeneity of a larger spatial scale, which in return would lead to an increase of the recommended size of the control volume. Based on the observed differences between the wind and temperature fields, it is conceivable that the space–time structure of other scalars such as humidity and carbon dioxide concentration will reveal more differences due to differences in their sinks and sources distribution and temporal dynamics in the canopy.
– Incorporating elements of the canopy and the terrain that contribute to within-domain heterogeneity into the sampling domain provides a framework to interpret spatial gradients and advective fluxes in the context of the site's heterogeneity and observed variability of the flow and scalar fields. Spatial temperature gradients and advective fluxes were sensitive to the choice of spatial interpolation algorithms, which may provide a perspective for a reinterpretation of existing studies.

Acknowledgements This research was in part supported by the Office of Science (BER), U.S. Department of Energy (DOE), contract DE-FG02-06ER64318. The valuable comments of Larry Mahrt, Dean Vickers, and three anonymous reviewers are greatly appreciated. The author wishes to thank James Liburdy for granting access to the wind-tunnel facilities. The author gratefully acknowledges the help of Kent Davis in collecting the field data and Garrett Meigs for extracting the Digital Elevation Model data, and the support of the AmeriFlux Qa/Qc laboratory of Beverly Law in providing reference instruments.

References

Anderson SP, Baumgartner MF (1998) Radiative heating errors in naturally ventilated air temperature measurements made from buoys. J Atmos Ocean Technol 15(1):157–173

Anfossi D, Oettl D, Degrazia G, Goulart A (2005) An analysis of sonic anemometer observations in low wind speed conditions. Boundary-Layer Meteorol 114(1):179–203

Aubinet M (2008) Eddy covariance CO_2 flux measurements in nocturnal conditions: an analysis of the problem. Ecol Appl 18(6):1368–1378

Aubinet M, Heinesch B, Yernaux M (2003) Horizontal and vertical CO_2 advection in a sloping forest. Boundary-Layer Meteorol 108(3):397–417

Aubinet M, Berbigier P, Bernhofer CH, Cescatti A, Feigenwinter C, Granier A, Grunwald TH, Havrankova K, Heinesch B, Longdoz B, Marcolla B, Montagnani L, Sedlak P (2005) Comparing CO_2 storage and advection conditions at night at different carboeuroflux sites. Boundary-Layer Meteorol 116(1):63–94

Aubinet M, Feigenwinter C, Heinesch B, Bernhofer C, Canepa E, Lindroth A, Montagnani L, Rebmann C, Sedlak P, van Gorsel E (2010) Direct advection measurements do not help to solve the night-time CO_2 closure problem: evidence from three different forests. Agric For Meteorol 150(5):655–664

Bohrer G, Katul GG, Walko RL, Avissar R (2009) Exploring the effects of microscale structural heterogeneity of forest canopies using large-eddy simulations. Boundary-Layer Meteorol 132(3):351–382

Feigenwinter C, Bernhofer C, Vogt R (2004) The influence of advection on the short term CO_2-budget in and above a forest canopy. Boundary-Layer Meteorol 113(2):201–224

Garratt JR (1980) Surface influence upon vertical profiles in the atmospheric near-surface layer. Q J R Meteorol Soc 106:803–819

Garratt JR (1992) The atmospheric boundary layer. Cambridge University Press, UK, 316 pp

Hanna SR (1986) Spectra of concentration fluctuations—the two time scales of a meandering plume. Atmos Environ 20(6):1131–1137
Heinesch B, Yernaux M, Aubinet M (2007) Some methodological questions concerning advection measurements: a case study. Boundary-Layer Meteorol 122(2):457–478
Heinesch B, Yernaux Y, Aubinet M (2008) Dependence of CO_2 advection patterns on wind direction on a gentle forested slope. Biogeoscience 5(3):657–668
Howell JF, Mahrt L (1997) Multiresolution flux decomposition. Boundary-Layer Meteorol 83:117–137
Lee XH, Hu XZ (2002) Forest-air fluxes of carbon, water and energy over non-flat terrain. Boundary-Layer Meteorol 103(2):277–301
Leuning R, Zegelin SJ, Jones K, Keith H, Hughes D (2008) Measurement of horizontal and vertical advectlion of CO_2 within a forest canopy. Agric For Meteorol 148(11):1777–1797
Mahrt L (2008) Mesoscale wind direction shifts in the stable boundary-layer. Tellus A 60(4):700–705
Mahrt L (2009) Characteristics of submeso winds in the stable boundary layer. Boundary-Layer Meteorol 130(1):1–14
Mahrt L, Thomas C, Prueger J (2009) Space-time structure of mesoscale modes in the stable boundary layer. Q J Roy Meteorol Soc 135:67–75
Mauder M, Desjardins RL, Gao Z, Van Haarlem R (2008) Errors of naturally ventilated air temperature measurements in a spatial observation network. J Atmos Ocean Technol 25(11):2145–2151
Moderow U, Feigenwinter C, Bernhofer C (2007) Estimating the components of the sensible heat budget of a tall forest canopy in complex terrain. Boundary-Layer Meteorol 123(1):99–120
Nakamura R, Mahrt L (2005) Air temperature measurement errors in naturally ventilated radiation shields. J Atmos Ocean Technol 22(7):1046–1058
Novak M, Warland J, Orchansky A, Kettler R, Green S (2000) Wind tunnel and field measurements of turbulent flow in forests. Part I: Uniformly thinned stands. Boundary-Layer Meteorol 95:457–495
Paw U KT, Baldocchi DD, Meyers TP, Wilson KB (2000) Correction of eddy-covariance measurements incorporating both advective effects and density fluxes. Boundary-Layer Meteorol 97(3):487–511
Poggi D, Porporato A, Ridolfi L, Albertson JD, Katul GG (2004) The effect of vegetation density on canopy sub-layer turbulence. Boundary-Layer Meteorol 111:565–587
Raupach MR, Thom A (1981) Turbulence in and above plant canopies. Annu Rev Fluid Mech 13:97–129
Staebler RM, Fitzjarrald DR (2004) Observing subcanopy CO_2 advection. Agric For Meteorol 122(3–4): 139–156
Staebler RM, Fitzjarrald DR (2005) Measuring canopy structure and the kinematics of subcanopy flows in two forests. J Appl Meteorol 44(8):1161–1179
Thomas C, Foken T (2007) Flux contribution of coherent structures and its implications for the exchange of energy and matter in a tall spruce canopy. Boundary-Layer Meteorol 123:317–337
Thomas C, Mayer JC, Meixner F, Foken T (2006) Analysis of low-frequency turbulence above tall vegetation using a Doppler sodar. Boundary-Layer Meteorol 119:563–587
Thomas C, Martin JG, Goeckede M, Siqueira MB, Foken T, Law BE, Loescher HW, Katul G (2008) Estimating daytime subcanopy respiration from conditional sampling methods applied to multi-scalar high frequency turbulence time series. Agric For Meteorol 148(8–9):1210–1229
Vickers D, Mahrt L (2006) Contrasting mean vertical motion from tilt correction methods and mass continuity. Agric For Meteorol 138:93–103
Whiteman CD, Hubbe JM, Shaw WJ (2000) Evaluation of an inexpensive temperature datalogger for meteorological applications. J Atmos Ocean Technol 17(1):77–81
Wilson KB, Baldocchi DD (2000) Seasonal and interannual variability of energy fluxes over a broadleaved temperate deciduous forest in North America. Agric For Meteorol 100(1):1–18
Wilson KB, Meyers TP (2001) The spatial variability of energy and carbon dioxide fluxes at the floor of a deciduous forest. Boundary-Layer Meteorol 98(3):443–473